PEFORMANCE OF TOUCHDOWN BEARINGS FOR TURBO MOLECULAR PUMPS

Yukio Ohura
NSK Ltd., Fujisawa, Kanagawa 251-8501 Japan
ooura@nsk.com

Kiyotoshi Ueda
NSK Ltd., Fujisawa, Kanagawa 251-8501 Japan
ueda-ki@nsk.com

Sumio Sugita
NSK Ltd., Fujisawa, Kanagawa 251-8501 Japan
sugita-s@nsk.com

ABSTRACT

Recently, high vacuum environments are required for various highly technical and precision industrial areas. A turbo molecular pump is a high vacuum device designed to achieve approximately 10^{-8}Pa, which consists of several components including high-speed magnetic bearings. In the event that electric power is cut off from the magnetic bearing for any unexpected reason, load capacity is immediately lost. The rotor and the stator then make contact with each other resulting in complete failure of the pump. In order to protect the pump and magnetic bearings, auxiliary landing bearings (touchdown bearings) are incorporated into the pump design. NSK investigated the shaft behavior of the pump, and by determining the amount of load applied to the bearing, we developed specifications for a more durable and thermal stress resistant auxiliary landing bearing.

INTRODUCTION

Whereas auxiliary bearings operate in a vacuum environment, the generated heat is difficult to diffuse, and the bearings are apt to have very localized hot spots. In addition, when the bearings are actually put into operation, they are exposed to severe load conditions due to shock load and abrupt acceleration [1]. As a result, any damaged bearings become extremely problematic. We have determined how to improve the durability of such bearings. Factors such as heat and load made things very complicated, so it was not enough for us to only understand probable causes of bearing failure. Accordingly, we tried to estimate bearing load by focusing on the behavior of the shaft and analyzing it to determine the amount of load it applies to the bearings. Based on our results, we have come to several significant conclusions related bearing specifications.

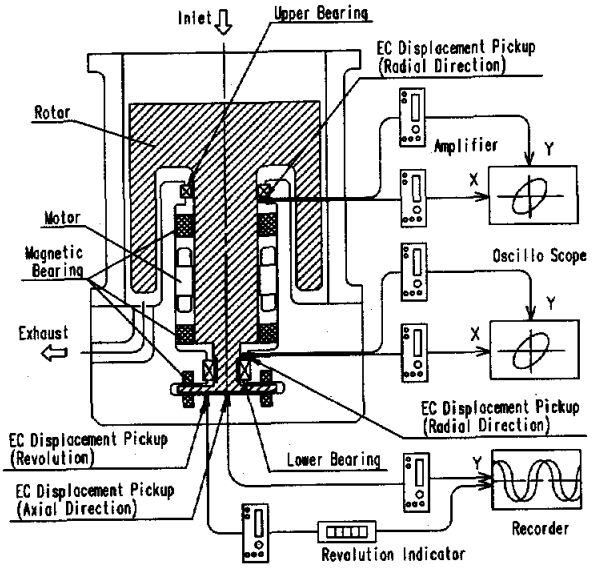

FIGURE 1: Structure of a turbo molecular pump

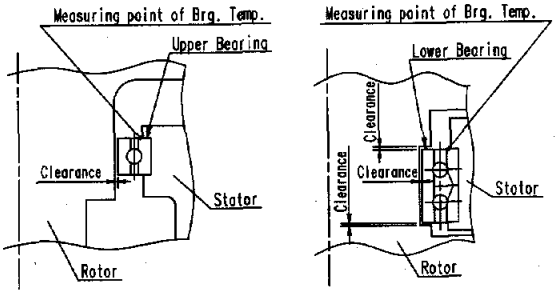

FIGURE 2: Area around of touchdown bearings

TABLE 1: Test conditions & tested bearings

Test conditions			Test bearings				
No.	Vacuum (Pa)	Rotating speed (rpm)	Position	Bore size (mm)	Type	Material	Coating
1	10^{-1}	21,600	Upper	Φ110	Full complement ball bearing (No cage)	Rings: SUS440C Balls: Si_3N_4	MoS_2 (Inner ring and balls)
			Lower	Φ60			
2		32,000	Upper	Φ60			
			Lower	Φ25			

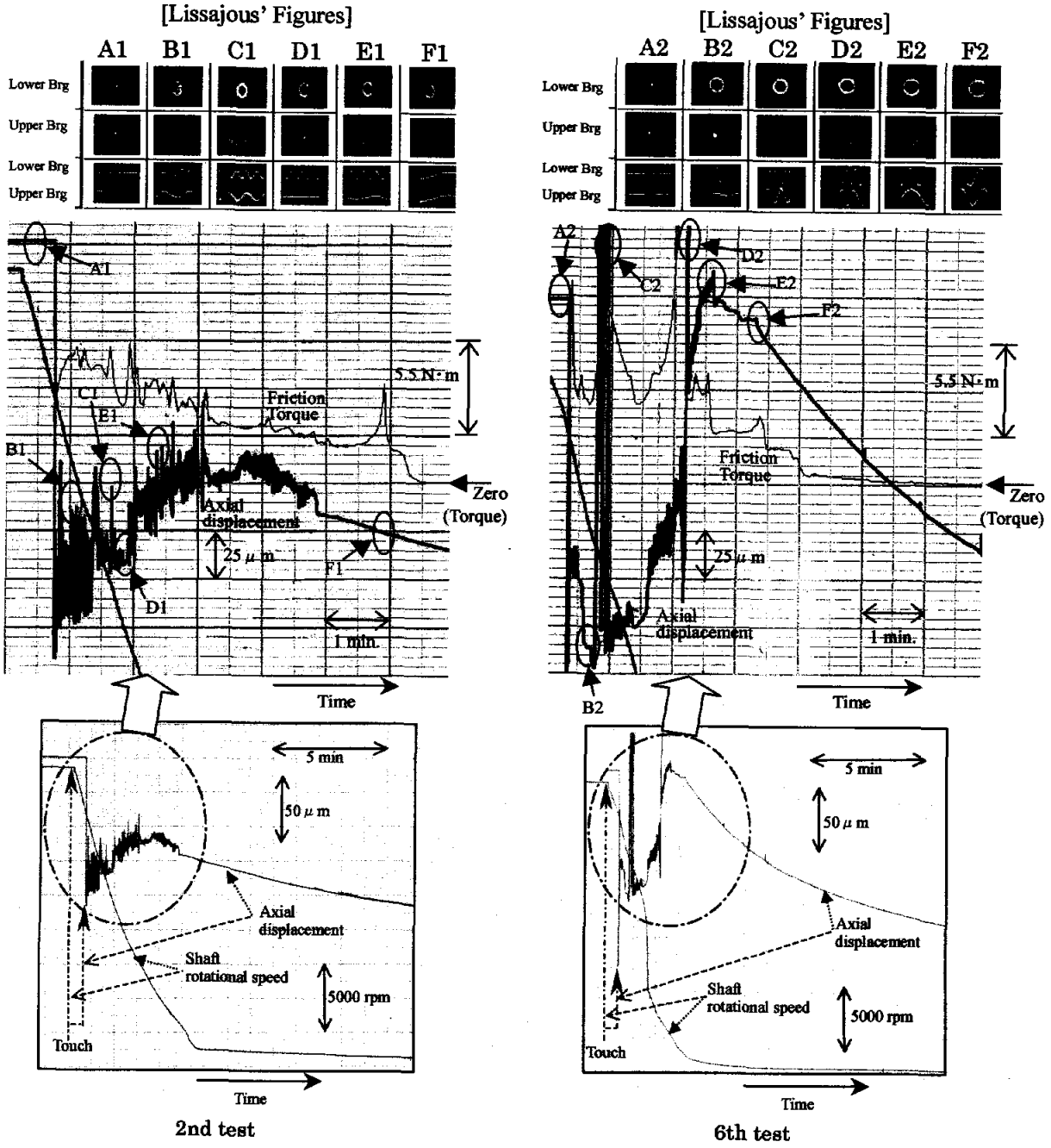

FIGURE 3: Experimental and calculated results

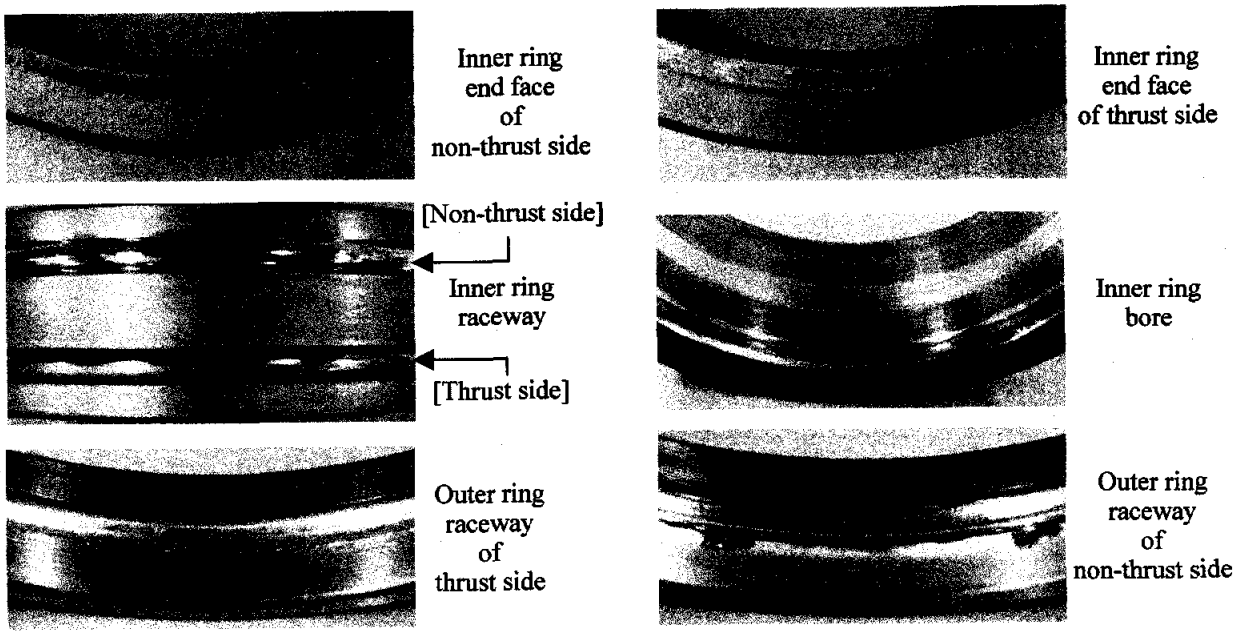

FIGURE 4-1: Lower bearing after test

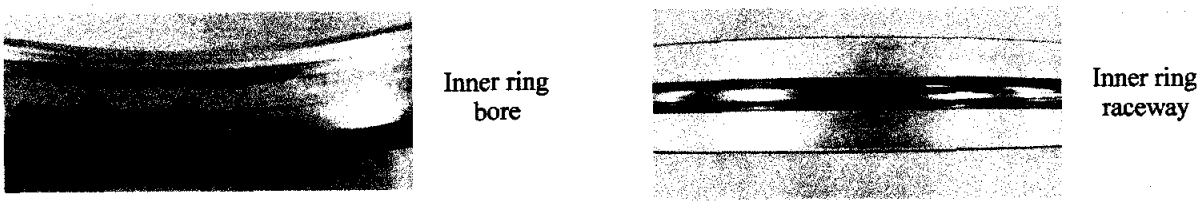

FIGURE 4-2: Upper bearing after test

LANDING TEST

Test method (Tests No. 1 & No. 2)

Test No. 1 (See TABLE 1) consisted of an actual pump, which was vertically mounted. The pump rotor was put into a delevitated coast down from the maximum rotating speed. This was repeated until abnormal signs of endurance, rotating speed, and sound appeared. Measured items consisted of shaft rotating speed, displacement of both upper and lower bearings in the radial direction, and axial displacement of the shaft. Figure 1 shows the locations of the sensors. Analysis of shaft behavior was completed only for the first test.

In Test No. 2 (See TABLE 1), the rotor of a different type of vertically mounted pump was delevitated at full speed. Outer ring temperatures of the upper and lower auxiliary bearings were measured. The positions of thermocouples are shown in Figure 2.

Test bearings

The axial clearance of the lower side auxiliary landing bearing in the first test was designed to be smaller than that of a standard bearing.

Test results

1) Shaft behavior

Axial displacement of the shaft, radial Lissajous, and changes in shaft rotating speed for the second and sixth trials respectively, are shown in Figure 3.

During the sixth trial, erratic bouncing of the shaft (vertical oscillation) was observed and found to be different from the type of bouncing that is normally found after delevitated coasting. Moderate movement of the shaft in an upward vertical direction was observed as well. Afterwards, the shaft continued to move upward until it could go no further.

2) Bearing appearance

Figure 4 shows damage to the bearing from the sixth trial. Inner and outer ring wear traces of the lower non-thrust side bearing were observed. Axial clearance increased to about 0.065 mm. Contact between both ends and the shaft within the bore diameter of the upper and lower bearings was strong. Slight scoring was also observed on the surface at the point of contact of the non-thrust-side lower bearing.

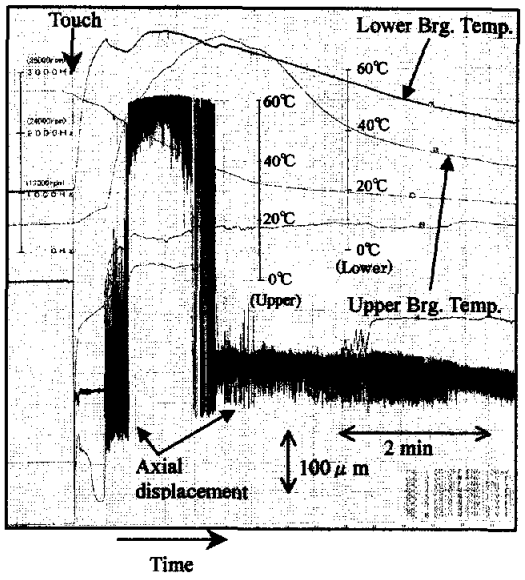

FIGURE 5: Experimental results (2)

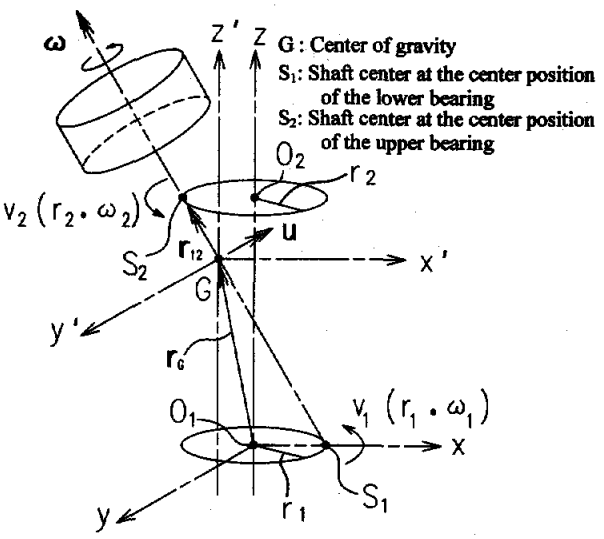

FIGURE 6: Coordinate system

3) Temperature

Figure 5 illustrates bearing temperature, and axial displacement of the pump used in test No. 2.

The sharp temperature rise of the upper bearing corresponds directly to when the shaft started bouncing, which continued for some time thereafter.

ANALYSIS

We determined that the shaft acts as a rotating element, moving in a gyroscopic manner, with a large amount of rotating energy, which is in unison with rectilinear movement. Accordingly, the coordinate system shown in Figure 6 shows that the bearing was incapable of sustaining moment load, and force in the z-axis direction was ignored. An equation of the shaft movement can be expressed as follows:

$$m\frac{d^2\mathbf{r}_G}{dt^2} = \mathbf{P}_1 + \mathbf{P}_2 \tag{1}$$

$$\frac{d\mathbf{H}_G}{dt} = \mathbf{M}_G \tag{2}$$

$$\mathbf{r}_{G1} \times \mathbf{P}_1 + \mathbf{r}_{G2} \times \mathbf{P}_2 = \mathbf{M}_G \tag{3}$$

$$\mathbf{H}_G = C\boldsymbol{\omega} + A\mathbf{u} \tag{4}$$

Here, u is a vector that crosses at right angles with ω and r_{12}, which is obtained from the following:

$$\mathbf{v}_2 = \mathbf{v}_1 + \mathbf{u} \times \mathbf{r}_{12} \tag{5}$$

$$\mathbf{u} \cdot \mathbf{r}_{12} = 0 \tag{6}$$

$$\left.\begin{aligned} \mathbf{v}_1 &= \left(-\omega_1 r_1 \sin\omega_1 t, \omega_1 r_1 \cos\omega_1 t, 0\right) \\ \mathbf{v}_2 &= \left(-\omega_2 r_2 \sin\omega_2 t, \omega_2 r_2 \cos\omega_2 t, \Delta v_z\right) \\ \Delta v_z &= \frac{r_1 r_2(\omega_1 - \omega_2)\sin\left((\omega_1 - \omega_2)t\right)}{\sqrt{L^2 - r_1^2 - r_2^2 + 2r_1 r_2 \cos\left((\omega_1 - \omega_2)t\right)}} \end{aligned}\right\} \tag{7}$$

Explanation of symbols

- m: Mass of the rotating element.
- $\mathbf{P}_1$, $\mathbf{P}_2$: Forces applied from the bearing to the shaft at S_1 and S_2 respectively.
- $\mathbf{H}_G$: Angular momentum of G.
- $\mathbf{M}_G$: Moment applied around G.
- A, C: Moment of inertia
- L: Distance between S_1 and S_2.

Therefore, when the data relating to r_1, r_2, ω_1, ω_2, and ω are obtained, radial loads $\mathbf{P}_1$ and $\mathbf{P}_2$, which are applicable to the bearing, can be determined. For the duration of calculation, r_1, r_2, ω_1, and ω_2 are regarded as being constant. The value of dω/dt was obtained by differentiating the data of ω, which is necessary to calculate the torque component of the rotating axis.

RESULT OF ANALYSIS

1) Torque (T)

Calculated torque (T) was added to the axial displacement data (See Figure 3). Changes in T and axial displacement synchronized very well. This was especially true during bouncing, where torque increased abruptly.

2) Loads applied to the bearing (P_1 and P_2)

Whereas torque applied to the bearing (T_b) can be expressed as $T_b=\mu \cdot d_m \cdot P$ (μ: friction coefficient; d_m: pitch circle diameter; P: radial load) [2], by assuming the friction coefficients of the upper and lower bearings to be constant and equal, the sum of bearing torque is proportional to $T_{cal}=d_{m1} \cdot P_1+d_{m2} \cdot P_2$.

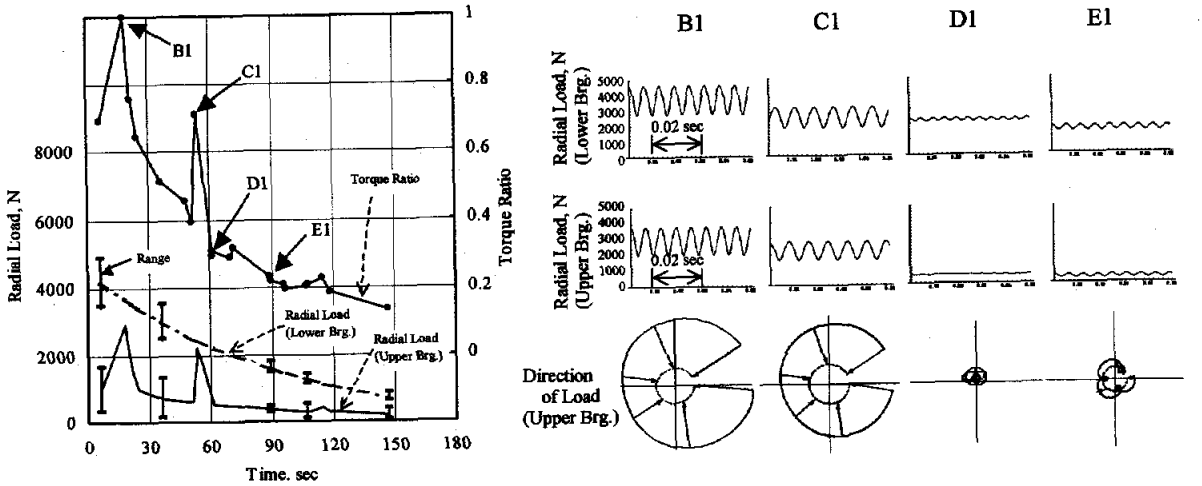

2nd test

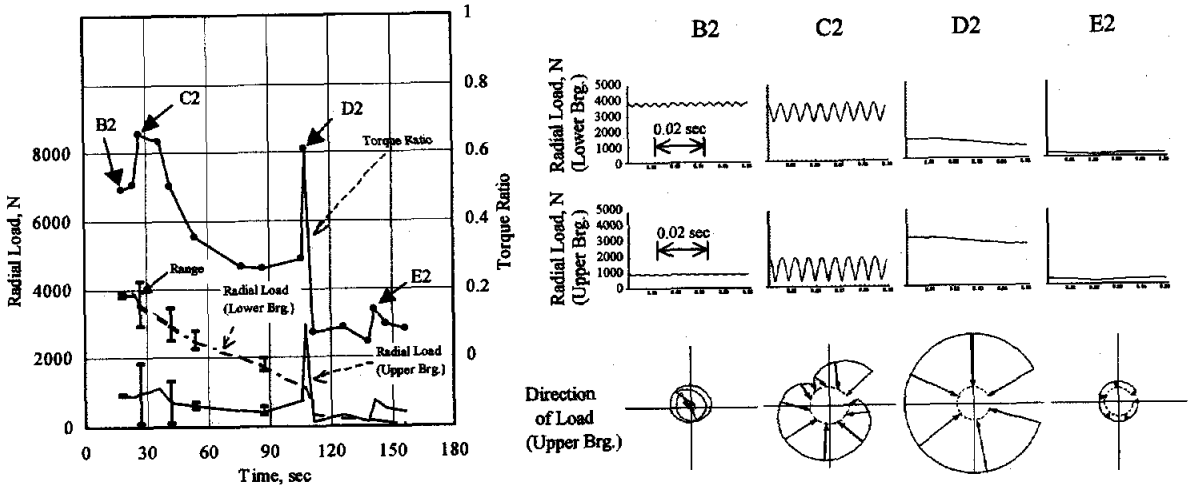

6th test

FIGURE 7: Analysis results

In Figure 7, based on T_{cal} of point B1, and by using the maximum value of P_1 and P_2, the ratio of T_{cal}, including time lapse, was plotted. Here, 1 and 2 indicate lower and upper bearings respectively. As a result, this data coincides with the tendency of torque (T) obtained from measured data. We are confident in the accuracy of P_1 and P_2, which was obtained from this analysis.

For a period of about 150 seconds we witnessed sudden bouncing and radial load being applied to the lower bearing, which is larger than the upper bearing (See Figures 3 & 7). However, during bouncing, which occurred during D2, load applied to the upper bearing was momentarily larger than that of lower bearing.

3) Axial displacement of the bearing

For the lower bearing, as internal clearance decreased due to heat generation, the shaft rose as shown in Figure 8. In the case of negative clearance, the shaft eventually rose at half of the amount of axial clearance (0.1 mm in this case), and maintained its position at that point, generating large internal load (See Figure 8).

CAUSE OF BOUNCING OF THE SHAFT AND SHAFT RISE

We determined that the "bounce force" was generated by frictional force generated through the large radial load acting between the shaft and the inner rings of the upper bearing from the following facts.

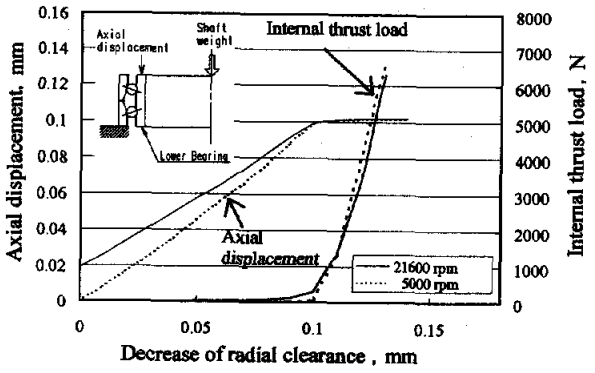

FIGURE 8: Relationships to axial displacement, internal thrust load and decrease of radial clearance

1) When bouncing occurred, the shaft entered a whirl with a large radius and a large radial load was generated, which was then applied to the upper bearing (See Figure 7).

2) When whirling was large, tilting at the contact area of the bearing also became large. Relative sliding velocity between the shaft and the inner ring acted in the upper vertical direction at the contact point.

3) When bouncing occurred, the temperature of the upper bearing also rose, which explained the large radial load that was being applied to upper bearing (See Figure 5).

4) Calculation

At the time of D2 (See Figure 3), where it seemed that the lower non-thrust side bearings were damaged, the friction force was calculated from the loads applied to the upper bearing and lower bearings (See Figure 7). For example, when we calculated the friction coefficient that occurred between the shaft and the inner ring of the bearing as 0.1 (MoS_2) [3], we were able to see generation of a thrust force that exceeded the weight of the shaft.

Alternatively, for moderate shaft rise, movement of the shaft was generated by the associated decrease of internal clearance of the bearing, which was due to heat generation that was caused by internal friction of the lower side bearing. The maximum rise of about 0.1 mm, as illustrated in Figure 8, coincided with the measured value illustrated in Figure 3. Data from the sixth trial (See Figure 3), after the rise of 0.1 mm, revealed a rise of about 0.075 mm that coincided with the increase of axial clearance of the lower bearing, which was caused by wear. Therefore, we concluded that shaft movement was a result of bearing wear.

CAUSE OF BEARING DAMAGE

Bouncing force was generated at the time of D2 as previously discussed. Meanwhile, Figure 8 shows that the bearing internal load increased considerably due to negative internal clearance of the lower bearing. We believe that overlapping of internal load and thrust force amplified the load that was applied to the non-thrust side of the lower bearing, and thus caused wear, which ultimately resulted in bearing failure.

BEARING SPECIFICATION

Important points for high performance bearings:

(a) A solid lubricant that can be utilized to reduce friction, and to maintain superior durability between the shaft and contact surfaces of the bearing

(b) For internal specifications, thermal resistance and rigidity measures must be considered:
- Low heat generation and seizure resistance
- Thermal balance of the inner rings, outer rings, and balls, which can thus minimize decreases of bearing internal clearance, and help maintain a stable clearance.
- Rigidity for resisting load and thermal stress

(c) Specification
- Application of MoS_2 coating on bearing surfaces
- Ceramic balls and application of MoS_2 coating on the balls and rings
- Optimization of bearing internal clearance including shaft and housing clearance
- Inner ring thicker than the outer ring (Upper and lower bearings) and inner ring with non separate type (Lower bearing)

CONCLUSION

By analyzing the behavior of the shaft, we were able to estimate the amount of load that was applied to the bearing. Utilizing the results, which have covered at this time, we hope to announce how to predict shaft behavior in the near future.

REFERENCES

1. Tessier L. P., The development of an auxiliary bearing landing system for a flexible AMB supported hydrogen process compressor rotor, Proc. of MAG'97, Alexandria, USA, Aug., 1997
2. Palmgren A., Grundlagen der Wälzlagertechnik, 1964.
3. Matsunaga M., Tsuya Y., Solid lubricant Handbook, 1982. (In Japanese)